# Dynamic in Situ Characterization of Organic Monolayer Formation via a Novel Substrate-Mediated Mechanism

Kevin S. Schneider,[†] Wei Lu,[‡] Daniel R. Fosnacht,[†] B. G. Orr,*[,§,||] and Mark M. Banaszak Holl*[,†,||]

*Chemistry Department, The University of Michigan, Ann Arbor, Michigan 48109-1055, Mechanical Engineering Department, The University of Michigan, Ann Arbor, Michigan 48109-2125, and Physics Department and the Applied Physics Program, The Harrison M. Randall Laboratory, The University of Michigan, Ann Arbor, Michigan 48109-1120*

*Received November 6, 2003*

**Ⓦ This paper contains enhanced objects available on the Internet at http://pubs.acs.org/journals/langd5.**

Ultrahigh vacuum scanning tunneling microscopy data investigating octylsilane ($C_8H_{17}SiH_3$) monolayer pattern formation on Au(111) are presented. The irregular monolayer pattern exhibits a 60 Å length scale. Formation of the octylsilane monolayer relaxes the Au(111) 23 × $\sqrt{3}$ surface reconstruction and ejects surface Au atoms. Au adatom diffusion epitaxially extends the Au(111) crystal lattice via step edge growth and island formation. The chemisorbed monolayer covers the entire Au surface at saturation exposure. Theoretical and experimental data suggest the presence of two octylsilane molecular adsorption phases: an atop site yielding a pentacoordinate Si atom and a surface vacancy site yielding a tetracoordinate Si atom. Theoretical simulations investigating two-phase monolayer self-assembly dynamics on a solid surface suggest pattern formation results from strain-induced spinodal decomposition of the two adsorption phases. Collectively, the theoretical and experimental data indicate octylsilane monolayer pattern formation is a result of interfacial Au−Si interactions and the alkyl chains play a negligible role in the monolayer pattern formation mechanism.

## 1. Introduction

Self-assembled monolayers have proven promising in a wide assortment of applications including chemical and biochemical sensing,[1,2] molecular electronic device fabrication,[3] nanopatterning, wetting control,[4,5] and corrosion inhibition.[6] To date, the vast majority of research investigating self-assembled monolayers (SAMs) explores the reactivity, properties, and utility of sulfur-containing molecules adsorbed on atomically flat Au(111) crystals, Au micro- and nanoparticles, and evaporated Au(111) surfaces.[6−9] Expansion and variation of the chemistry present at the SAM interface, in particular the substrate/headgroup interaction, may significantly alter the chemical, physical, and electronic properties of these versatile materials. In this paper, we explore the effect of a trivalent silicon headgroup upon the nature of the patterning, including both the periodicity and length scales, associated with SAM formation.

Silicon-based monolayers have provided an important alternative to sulfur-based SAMs for nearly 30 years. Through the utilization of octadecyltrichlorosilane ($C_{18}H_{37}SiCl_3$) to form monolayers on oxidized aluminum, oxidized silicon, and glass substrates, Sagiv et al. provided the first comprehensive set of experiments describing formation of alkane monolayers containing silicon headgroups.[10−17] Subsequently, Rubinstein and Sagiv, as well as Finklea and Allara, expanded this work to gold surfaces.[18,19] In 1989, Whitesides and co-workers investigated alkylsiloxane ($RSiO_3$) and alkyltrichlorosilane ($RSiCl_3$) SAMs on oxidized Si substrates.[20,21] Shortly thereafter, Ulman explored the potential optoelectronic and molecular electronic utility of these materials.[22] Nuzzo, Dubois, and co-

[†] Chemistry Department, The University of Michigan.
[‡] Mechanical Engineering Department, The University of Michigan.
[§] Physics Department, The Harrison M. Randall Laboratory, The University of Michigan.
[||] Applied Physics Program, The Harrison M. Randall Laboratory, The University of Michigan.

(1) Crooks, R. M.; Ricco, A. J. *Acc. Chem. Res.* **1998**, *31*, 219−227.
(2) Chaki, N. K.; Vijayamohanan, K. *Biosens. Bioelectron.* **2002**, *17*, 1−12.
(3) Tour, J. M.; Jones, L., II; Pearson, D. L.; Lamba, J. J. S.; Burgin, T. P.; Whitesides, G. M.; Allara, D. L.; Parikh, A. N.; Atr, S. V. *J. Am. Chem. Soc.* **1995**, *117*, 9529−9534.
(4) Laibinis, P. E.; Bain, C. D.; Nuzzo, R. G.; Whitesides, G. M. *J. Phys. Chem.* **1995**, *99*, 7663−7676.
(5) Shon, Y.-S.; Lee, S.; Colorado, J., R.; Perry, S. S.; Lee, T. R. *J. Am. Chem. Soc.* **2000**, *122*, 7556−7563.
(6) Ulman, A. *Chem. Rev.* **1996**, *96*, 1533−1554.
(7) Nuzzo, R. G.; Allara, D. L. *J. Am. Chem. Soc.* **1983**, *105*, 4481−4483.
(8) Poirier, G. E. *Chem. Rev.* **1997**, *97*, 1117−1127.
(9) Schreiber, F. *Prog. Surf. Sci.* **2000**, *65*, 151−257.
(10) Polymeropoulos, E. E.; Sagiv, J. *J. Chem. Phys.* **1978**, *69*, 1836−1847.
(11) Gun, J.; Iscovici, R.; Sagiv, J. *J. Colloid Interface Sci.* **1984**, *101*, 201−213.
(12) Maoz, R.; Sagiv, J. *J. Colloid Interface Sci.* **1984**, *100*, 465−496.
(13) Netzer, L.; Iscovici, R.; Sagiv, J. *Thin Solid Films* **1983**, *100*, 67−76.
(14) Netzer, L.; Iscovici, R.; Sagiv, J. *Thin Solid Films* **1983**, *99*, 235−241.
(15) Sagiv, J. *Isr. J. Chem.* **1979**, *18*, 339−345.
(16) Sagiv, J. *Isr. J. Chem.* **1979**, *18*, 346−353.
(17) Sagiv, J. *J. Am. Chem. Soc.* **1980**, *102*, 92−98.
(18) Sabatani, E.; Rubinstein, I.; Maoz, R.; Sagiv, J. *J. Electroanal. Chem.* **1987**, *219*, 365−371.
(19) Finklea, H. O.; Robinson, L. R.; Blackburn, A.; Richter, B.; Allara, D.; Bright, T. *Langmuir* **1986**, *2*, 239−244.
(20) Wasserman, S. R.; Whitesides, G. M.; Tidswell, I. M.; Ocko, B. M.; Pershan, P. S.; Axe, J. D. *J. Am. Chem. Soc.* **1989**, *111*, 5852−5861.
(21) Wasserman, S. R.; Tao, Y. T.; Whitesides, G. M. *Langmuir* **1989**, *5*, 1074−1087.
(22) Ulman, A. *Adv. Mater.* **1990**, *2*, 573−582.

10.1021/la0360916 CCC: $27.50 
Published on Web 01/07/2004

workers,[23−26] along with Goodman et al.,[27,28] greatly expanded the chemistry of silicon-based SAMs via formation of silicide and organosilane ($RSiH_3$) monolayers on a variety of oxidized and unoxidized metal surfaces including Cu(111), Ni(100), Ni(111), and W(110). Interestingly, Nuzzo demonstrated the first example of Si−H bond activation by a metal surface via chemisorption of primary organosilanes ($RSiH_3$) on Cu(111) to form surface-bound silylyne units ($RSi\equiv$).[26]

Ambient temperature Si−H bond activation by gold was first observed in 1999 via chemisorption of $H_8Si_8O_{12}$ spherosiloxane clusters to Au(111).[29] This discovery set the stage for a novel class of silicon-based monolayers on Au. In the past year, our group has synthesized and characterized *n*-hexylsilane ($C_6H_{13}SiH_3$), *n*-octylsilane ($C_8H_{17}SiH_3$), and *n*-octadecylsilane ($C_{18}H_{37}SiH_3$) monolayers on freshly evaporated Au(111) surfaces.[30,31] X-ray photoemission spectroscopy (XPS) and reflection absorption infrared spectroscopy (RAIRS) indicate alkylsilanes chemisorb to Au(111) via activation of the three Si−H bonds, leaving the molecule standing upright on the substrate.[30] The resulting alkylsilane monolayers are stable to prolonged exposures of $H_2O$, $O_2$, and X-ray irradiation in ultrahigh vacuum, although they readily oxidize upon exposure to ambient atmosphere.[30] The oxidized alkylsilane monolayers exhibit significantly enhanced stability—relative to their oxidized alkanethiol counterparts[32]—to solvent rinses (water, methanol, and *n*-hexane).

A recent scanning tunneling microscopy (STM) and XPS investigation of the octylsilane ($C_8H_{17}SiH_3$) monolayer prior to and following ambient atmosphere oxidation yielded intriguing chemical and physical phenomena.[33] However, a thorough examination of the dynamics and length scales involved with monolayer formation has not been presented. In this paper, comprehensive in situ STM data examining the dynamics of octylsilane monolayer and accompanying pattern formation mechanisms on Au(111) $23 \times \sqrt{3}$ are presented. Octylsilane monolayer formation relaxes the Au(111) $23 \times \sqrt{3}$ surface reconstruction, resulting in ejection of surface Au atoms and formation of Au islands. STM movies are presented dramatically displaying both Au island formation and roughening of Au(111) substrate terrace edges. At saturation coverage, the stable Au islands and terrace edges are uniformly covered underneath the octylsilane monolayer.

The headgroup-induced changes in the nature of the ordering for the octylsilane monolayer, relative to the octanethiol SAM analogue, are dramatic. Previous STM studies of the octanethiol SAM adsorbed on Au(111) have illustrated a 5 Å hexagonal packing.[8,34] Curiously, this repeat distance has proven invariant to a dramatic change in headgroup as exemplified by the work of Fichou et al. employing $-SiMe_3$.[35,36] However, the trivalent RSi headgroup featured in this paper yields a monolayer pattern lacking the hexagonal packing and feature dimensions of the previous two systems. Instead, the octylsilane monolayer pattern includes a characteristic length scale of ∼60 Å, dramatically different from that previously observed in the alkanethiol SAM system and unique to the field of chemisorbed organic layers on surfaces.

The physical origin of the octylsilane monolayer pattern, with a length scale roughly 6 times the size of the molecules employed and 20 times the Au−Au distance, results from surface Au−Si interactions. A combination of theoretical and experimental data suggests the complex octylsilane monolayer pattern results from strain-mediated spinodal decomposition of two different molecular adsorption phases. To date, monolayer pattern formation via spinodal decomposition has not been observed for organization of organic monolayers on surfaces.

The importance of these fundamental studies is best understood in the context of the rapid development in the past 5 years of the field of alkysilane-based monolayers, in terms of both basic science and potential applications. Briefly, Fadeev and co-workers have investigated the synthesis and properties of covalently attached monolayers via chemisorption of alkylsilanes, alkylsiloxanes, and alkylchlorosilanes to a variety of oxidized transition metal and silica surfaces.[37−41] Through their extensive work, Fadeev et al. have greatly expanded the chemical palette available for molecular modification of surfaces.

Concurrently to our work developing alkylsilane monolayers on gold, Fichou and co-workers have reported the long-range self-assembly of trimethylsilylacetylene monolayers on Au(111).[35,36] In their studies, Fichou et al. employed STM to provide the first compelling evidence of self-assembly of silicon-based monolayers on Au.

A dramatic application of alkylsilane monolayers on gold was recently demonstrated by Klabunde, Sorensen, et al. via the use of gold nanoparticles to oxidatively polymerize alkylsilanes to form nanoscale siloxane wires, filaments, and tubes.[42] This unique application of alkylsilane monolayers, building upon our earlier work demonstrating both that they could be made and that Si−H bond activation by gold was facile, highlights the importance of developing novel monolayer systems with alternative headgroups. In addition, the work highlights the importance of understanding the alkylsilane monolayer packing and density considering the potential influence these parameters may have on the nanoscale structure of the siloxane materials generated.

## 2. Experimental Details

*n*-Octylsilane ($CH_3(CH_2)_7SiH_3$) was purchased from Gelest, Inc., and loaded into a glass ultrahigh vacuum (UHV) compatible container. Prior to experimental use, the sample was further purified by multiple freeze−pump−thaw cycles.

(23) Nuzzo, R. G.; Dubois, L. H. *Surf. Sci.* **1985**, *149*, 119−132.
(24) Dubois, L. H.; Nuzzo, R. G. *Surf. Sci.* **1985**, *149*, 133−145.
(25) Wiegand, B. C.; Lohokare, S. P.; Nuzzo, R. G. *J. Phys. Chem.* **1993**, *97*, 11553−11562.
(26) Hostetler, M. J.; Nuzzo, R. G.; Girolami, G. S. *J. Am. Chem. Soc.* **1994**, *116*, 11608−11609.
(27) Sault, A. G.; Goodman, D. W. *J. Catal.* **1990**, *126*, 57−72.
(28) Sault, A. G.; Goodman, D. W. *Surf. Sci.* **1990**, *235*, 28−46.
(29) Nicholson, K. T.; Zhang, K. Z.; Banaszak Holl, M. M. *J. Am. Chem. Soc.* **1999**, *121*, 3232−3233.
(30) Owens, T. M.; Nicholson, K. T.; Banaszak Holl, M. M.; Süzer, S. *J. Am. Chem. Soc.* **2002**, *124*, 6800−6801.
(31) Owens, T. M.; Süzer, S.; Banaszak Holl, M. M. *J. Phys. Chem. B* **2003**, *107*, 3177−3182.
(32) Schoenfisch, M. H.; Pemberton, J. E. *J. Am. Chem. Soc.* **1998**, *120*, 4502−4513.
(33) Schneider, K. S.; Owens, T. M.; Fosnacht, D. R.; Orr, B. G.; Banaszak Holl, M. M. *ChemPhysChem* **2003**, *10*, 1111−1114.
(34) Poirier, G. E.; Tarlov, M. J. *Langmuir* **1994**, *10*, 2853−2856.
(35) Marchenko, A.; Katsonis, N.; Fichou, D.; Aubert, C.; Malacria, M. *J. Am. Chem. Soc.* **2002**, *124*, 9998−9999.
(36) Katsonis, N.; Marchenko, A.; Taillemite, S.; Fichou, D.; Chouraqui, G.; Aubert, C.; Malacria, M. *Chem. Eur. J.* **2003**, *9*, 2574−2581.
(37) Fadeev, A. Y.; McCarthy, T. J. *J. Am. Chem. Soc.* **1999**, *121*, 12184−12185.
(38) Cao, C. T.; Fadeev, A. Y.; McCarthy, T. J. *Langmuir* **2001**, *17*, 757−761.
(39) Fadeev, A. Y.; Kazakevich, Y. V. *Langmuir* **2002**, *18*, 2665−2672.
(40) Helmy, R.; Fadeev, A. Y. *Langmuir* **2002**, *18*, 8924−8928.
(41) Marcinko, S.; Helmy, R.; Fadeev, A. Y. *Langmuir* **2003**, *19*, 2752−2755.
(42) Prasad, B. L. V.; Stoeva, S. I.; Sorensen, C. M.; Zaikovski, V.; Klabunde, K. J. *J. Am. Chem. Soc.* **2003**, *125*, 10488−10489.

Clean Au(111) samples for STM imaging experiments were prepared by one of two methods. The first method entailed annealing a commercially fabricated sample of Au deposited on mica (Molecular Imaging) in UHV (base pressure $5 \times 10^{-11}$ Torr). Sample annealing was accomplished by resistively heating to ~673−773 K (temperature measured with a Minolta-Land infrared optical pyrometer; Cyclops 52, emissivity setting 0.7) a ~3 mm × 5 mm × 0.3 mm piece of oxidized Si(100) cut from a larger wafer (Virginia Semiconductor, p-type, B-doped, resistivity ~0.003 Ω·cm) situated directly underneath the mica. In a separate chamber (base pressure $3 \times 10^{-10}$ Torr), gold (99.999% vacuum deposition grade, Cerac, Inc., placed inside a coiled 0.01 in. W wire tungsten filament; California Fine Wire) was deposited on the surface for ~40 min at an approximate rate of 1 Å/s (film thickness determined by atomic force microscopy). Following Au deposition, the sample was further annealed (typically 3 h). Samples prepared in this manner were not removed from UHV prior to experimentation. The second method involved thermal evaporation of Au onto clean mica in UHV. Immediately prior to Au evaporation, freshly cleaved mica (Asheville-Schoonmaker, research grade high-quality mica) was degassed overnight (>12 h) in UHV (base pressure $5 \times 10^{-11}$ Torr) at ~673 K. Sample heating was accomplished by resistively heating a ~3 mm × 5 mm × 0.3 mm piece of oxidized Si(100) cut from a larger wafer situated directly underneath the mica. In a separate chamber, gold was deposited on the surface for ~40 min at an approximate rate of 1 Å/s. Following Au evaporation, the sample was annealed at ~673−773 K for at least 1 h. After annealing, the Au sample had to be removed from UHV for installation into the STM sample holder. The Au sample was exposed to ambient atmosphere for ~6.5 min before it was placed into a load lock and pumped down for 30 min to a pressure of $\sim 1 \times 10^{-7}$ Torr. Upon reentry into UHV, the Au sample was further annealed for at least 1 h. Prior to octylsilane adsorption, Au samples prepared using both methods were first imaged in UHV (base pressure $5 \times 10^{-11}$ Torr) by STM in order to assess the sample structure and confirm the presence of the Au(111) $23 \times \sqrt{3}$ surface reconstruction.

Gaseous octylsilane was introduced into the UHV chamber via a leak valve. Room-temperature Au(111) $23\times \sqrt{3}$ samples were exposed to octylsilane dosing pressures between $1 \times 10^{-8}$ and $1 \times 10^{-6}$ Torr.

UHV-STM images were acquired at room temperature in the constant-current mode using an RHK Technology, Inc., UHV300 series variable-temperature scanning tunneling microscope at typical sample biases ($V_S$) of ±0.5−1.0 V and tunneling currents ($I_T$) of 0.01−2.0 nA. Commercially fabricated platinum/iridium (80/20) STM tips (Materials Analytical Services, "Controlled Geometry" Pt/Ir STM tips) were used for imaging. Radiative tip cleaning was accomplished by holding the tip directly above a Si(100) sample (outside of tunneling range) heated to ~1173 K for 10−20 min prior to imaging. Low and/or high pass filters were employed to attenuate extraneous $I_T$ noise in the STM images.

Theoretical simulations were performed to investigate two-phase monolayer self-assembly dynamics on a solid surface. Complete quantitative details of the simulation theory and methods employed are fully described elsewhere and are briefly summarized here.[43−45] A value of $E \sim 7.8 \times 10^{10}$ N/m$^2$ was employed for the elastic modulus of gold and $h_0 \sim 10^{-19}$ J for the binding energy between the phases. Two competing actions determine the monolayer patterns. The phase boundary energy drives phase coarsening. The concentration-dependent surface stress drives phase refining. Competition between the coarsening and the refining leads to size selection and spatial ordering. The simulation method embodies these thermodynamic forces in a nonlinear diffusion equation. Previous simulations focused on the annealing process in which the average concentration of the two phases is invariant.[43−45] However, in the simulation presented here, the deposition process is incorporated into the model, thereby allowing the average concentration of the two phases to change upon deposition. Mechanics level computations to crudely assess the bond lenths and angles of several possible bonding modes were performed using Spartan '02, Wavefunction, Inc., Irvine, CA.

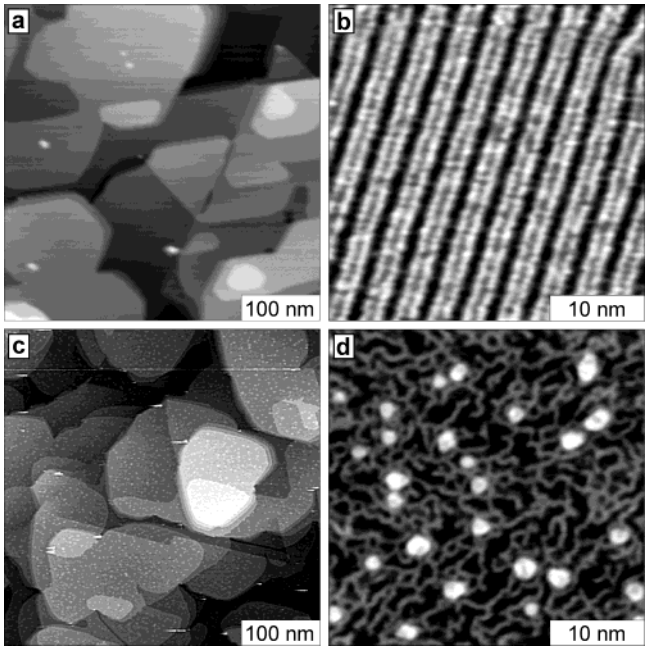


**Figure 1.** (a) A large area (4000 Å × 4000 Å) STM image of clean Au(111): $V_S = -0.50$ V, $I_T = 1.25$ nA. (b) A high resolution (350 Å × 350 Å) STM image of clean Au(111): $V_S = -0.99$ V, $I_T = 0.20$ nA. (c) A 4000 Å × 4000 Å STM image of the monolayer formed from exposure of Au(111) to 50 langmuirs of gaseous octylsilane: $V_S = -1.03$ V, $I_T = 0.64$ nA. (d) A 350 Å × 350 Å STM image of the monolayer formed from exposure of Au(111) to 50 langmuirs of gaseous octylsilane: $V_S = -1.00$ V, $I_T = 0.26$ nA. The Au(111) sample in (c) and (d) had not been exposed to ambient atmosphere prior to octylsilane adsorption.

## 3. Results

**3.1. Analysis of the Octylsilane Monolayer.** A large scale (4000 Å × 4000 Å) STM image of a typical clean Au sample prepared in either of the manners previously described displays gold terraces ranging in size from hundreds to several thousand angstroms (Figure 1a). Cross-sectional analyses of the substrate terraces exhibit the Au single-step height of ~2.5 Å. A high-resolution image (350 Å × 350 Å) of the Au sample clearly displays the parallel striped features intrinsic to the Au(111) $23 \times \sqrt{3}$ surface reconstruction (Figure 1b).[46−50] Exposure of the clean Au(111) surface to a saturating dose of gaseous octylsilane in UHV (≤50 langmuirs for a Au(111) sample that has not been exposed to ambient atmosphere prior to octylsilane exposure in UHV and >300 langmuirs for a sample that has been exposed to ambient atmosphere prior to octylsilane exposure in UHV; 1 langmuir = $1 \times 10^{-6}$ Torr·s) yields dramatic changes in the sample surface topography. A large area (4000 Å × 4000 Å) STM image of the octylsilane monolayer displays Au terraces mottled with numerous, small surface protrusions (Figure 1c). Close inspection of Figure 1c reveals rounded and jagged

(43) Suo, Z.; Lu, W. *J. Nanopart. Res.* **2000**, *2*, 333−344.
(44) Lu, W.; Suo, Z. *Phys. Rev. B* **2002**, *65*, 085401.
(45) Lu, W.; Suo, Z. *Phys. Rev. B* **2002**, *65*, 205418.
(46) Van Hove, M. A.; Koestner, R. J.; Stair, P. C.; Bibérian, J. P.; Kresmodel, L. L.; Bartoš, I.; Somorjai, G. A. *Surf. Sci.* **1981**, *103*, 189−217.
(47) Harten, U.; Lahee, A. M.; Toennies, J. P.; Wöll, C. *Phys. Rev. Lett.* **1985**, *54*, 2619−2622.
(48) Wöll, C.; Chiang, S.; Wilson, R. J.; Lippel, P. H. *Phys. Rev. B* **1989**, *39*, 7988−7991.
(49) Barth, J. V.; Brune, H.; Ertl, G.; Behm, R. J. *Phys. Rev. B* **1990**, *42*, 9307−9318.
(50) Chambliss, D. D.; Wilson, R. J.; Chiang, S. *J. Vac. Sci. Technol., B* **1991**, *9*, 933−937.

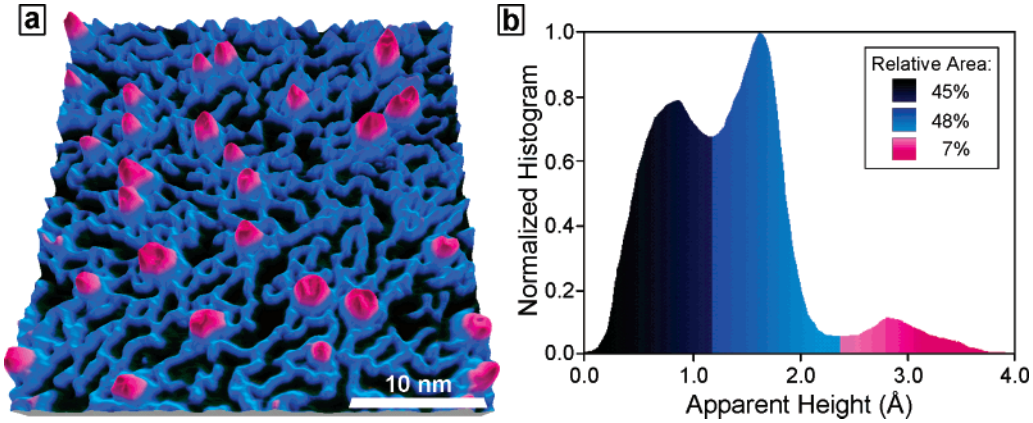


**Figure 2.** (a) A height-mapped surface rendering (350 Å × 350 Å) of Au(111) 23 × √3 sample exposed to 50 langmuirs of octylsilane (the Au(111) substrate was not exposed to ambient atmosphere prior to octylsilane exposure): $V_S = -1.00$ V, $I_T = 0.26$ nA. The image is false-colored to best differentiate the monolayer features. (b) A normalized height histogram of the image presented in part a.

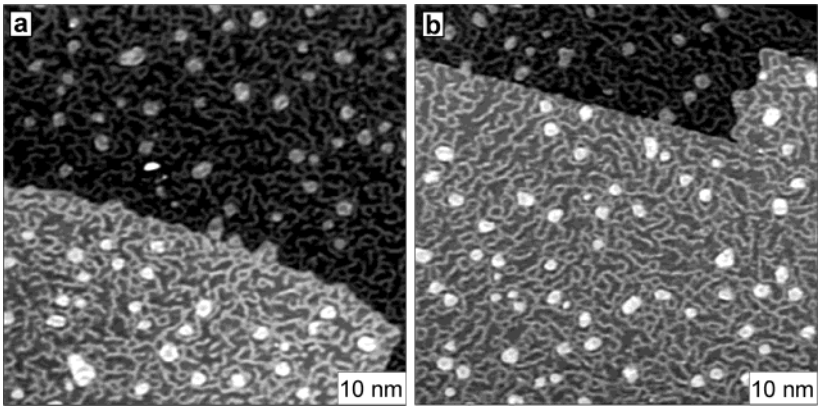


**Figure 3.** Octylsilane monolayer formed from exposure of Au(111) to 50 langmuirs of gaseous octylsilane in UHV (600 Å × 600 Å, the Au(111) sample was not exposed to ambient atmosphere prior to octylsilane exposure). The images clearly show roughened step edge features associated with monolayer formation. (a) $V_S = -1.00$ V, $I_T = 0.42$ nA. (b) $V_S = -1.01$ V, $I_T = 0.39$ nA.

Au terrace edges with small lateral, fingerlike protrusions emanating from step edges. A high-resolution image (350 Å × 350 Å) of a single terrace of the octylsilane monolayer displays a complex pattern of surface features (Figure 1d). The octylsilane monolayer surface is characterized by an interwoven pattern of elevated sinuous ridges that frequently combine to form looped or knotted features. The ridges are approximately 0.8 Å high relative to the surrounding darkly contrasted depressed regions and approximately 10 Å in apparent width. Additionally, there are numerous brightly contrasted interstitial hillock features 20−40 Å in diameter and ∼2.5 Å in apparent height relative to the depressed regions. The apparent height of a hillock feature is equivalent to and indistinguishable from that of a single-step Au terrace. Close inspection of the hillock features in Figure 1d and subsequent images reveal a similar texture (i.e., elevated sinuous ridges) as the surrounding monolayer surface. Apparent heights of the octylsilane monolayer features do not vary significantly with changes in tunneling current (10 pA−2 nA) or applied sample bias (±2 V).

Analysis of STM image height histograms provides quantitative information of the octylsilane monolayer surface features. A false-colored 350 Å × 350 Å STM image of the octylsilane monolayer is displayed in Figure 2a. The colors have been chosen to best visually differentiate the three distinct monolayer surface features. Height histograms plot STM data in the form of pixel color frequency versus apparent height to produce a curve. This curve can be decomposed into broadened levels to indicate regions of equivalent apparent height. Integration of individual level curves yields surface coverage values for the corresponding features at specific heights. A normalized height histogram of the STM image in Figure 2a is presented in Figure 2b. The darkest contrasted regions of the histogram have been arbitrarily set to zero. In Figure 2a, the black regions and surrounding blue sinuous ridges comprise nearly equivalent amounts of the STM image (45% and 48%, respectively). This relative amount of surface feature composition is nominally observed for all STM images of the octylsilane monolayer with approximately ±10% variability from image to image. The red interstitial hillock features cover approximately 7% of the monolayer surface in Figure 2a. The hillock features typically exhibit a surface coverage area range of 4−10% in the STM images.

High-resolution images of the octylsilane monolayer spanning multiple terraces clearly display the textured features of the terrace edges faintly visible in larger area images (Figure 3). Terrace edge textures range from jagged features (Figure 3a) to smooth, rounded features (Figure 3b). Interestingly, Figure 3b contains a terrace edge that is predominantly straight and smooth (running diagonally down from the top left corner of the image) and one that is dramatically rounded (top right portion of the image).

Current versus voltage ($I-V$) scanning tunneling spectroscopy (STS) data acquired simultaneously during acquisition of STM topographic images yield no significant differences in the electronic signatures of the hillock and surrounding monolayer features.

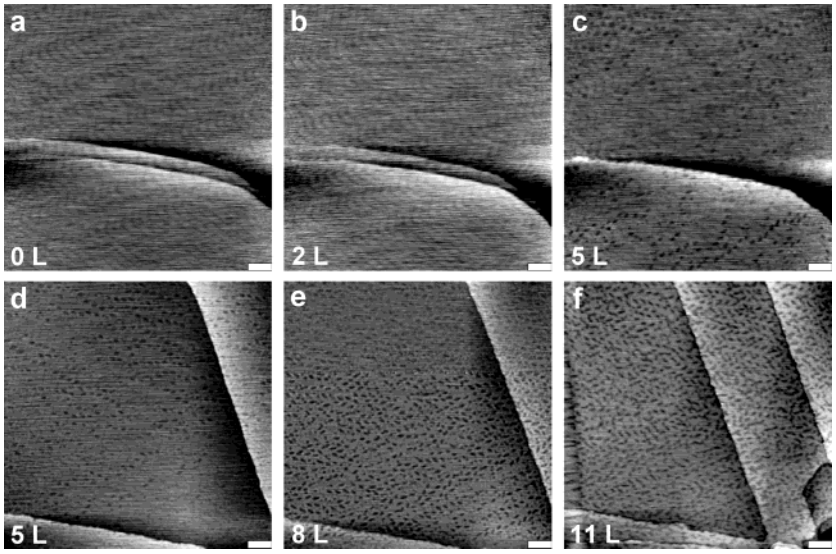


**Figure 4.** Incremental in situ UHV-STM images of Au(111) as a function of increasing octylsilane exposure (indicated in the lower left corner). The Au(111) sample was exposed to ambient atmosphere ~6.5 min prior to octylsilane exposure. All images are 1220 Å × 1220 Å in area and were acquired with $V_S = -1$ V and $I_T = 7-30$ pA. The white scale bar in the bottom right corner of each image signifies 100 Å.

Ⓦ STM animations showing increasing octylsilane exposure, Ⓦ 0 to 5 langmuirs and Ⓦ 5 to 11 langmuirs, in GIF format are available.

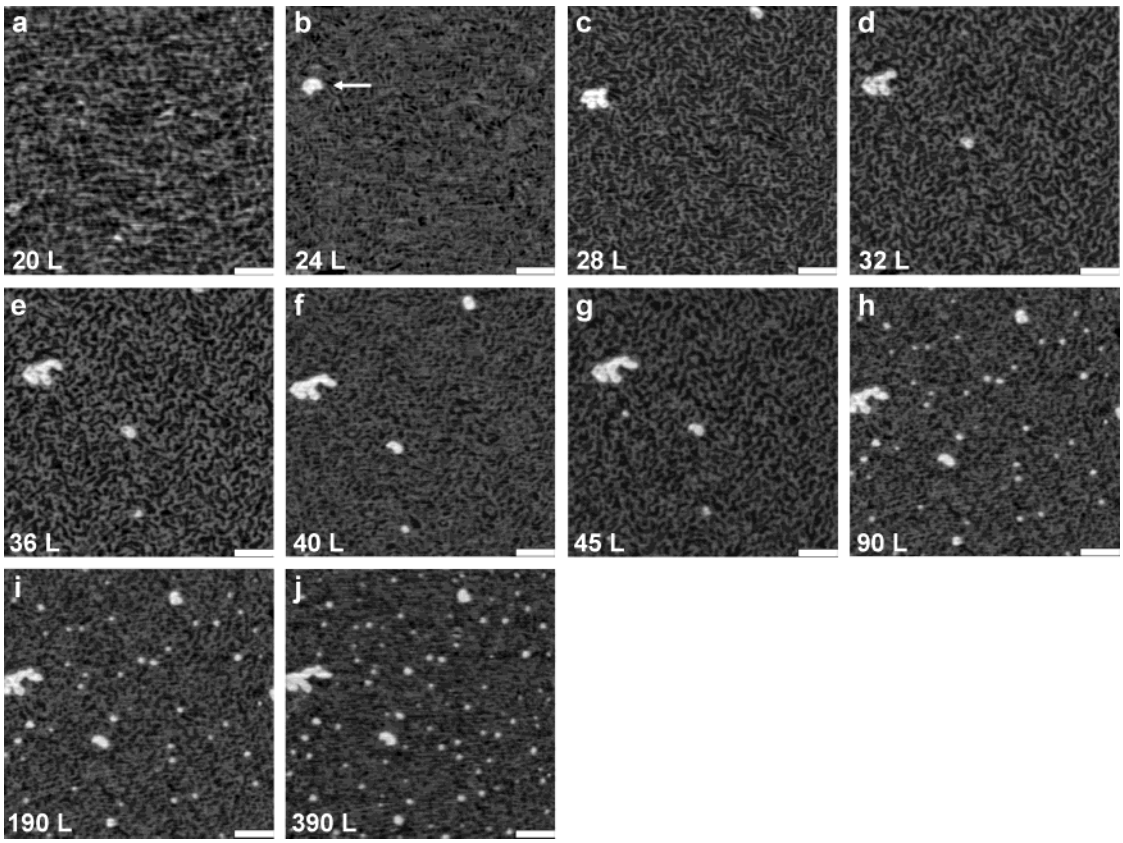


**Figure 5.** Incremental in situ UHV-STM images of a single Au(111) terrace as a function of increasing octylsilane exposure (indicated in the lower left corner). The Au(111) sample was exposed to ambient atmosphere ~6.5 min prior to octylsilane exposure. All images are 710 Å × 710 Å in area and were acquired with $V_S = -1$ V and $I_T = 15-40$ pA. The white scale bar in the bottom right corner of each image signifies 100 Å.

Ⓦ A STM animation showing increasing octylsilane exposure, 20 to 390 langmuirs, in GIF format is available.

**3.2. Evolution of Octylsilane Monolayer Features.** To best interpret the origin of the octylsilane monolayer features, in situ UHV-STM imaging experiments monitoring sequential changes in substrate features as a function of increasing octylsilane exposure have been performed. The data collected have been compiled in movie format. Static snapshots taken from the STM movies are presented in Figures 4 and 5 for representative octylsilane exposure amounts (in langmuirs); however, the data is best viewed dynamically in movie format. As previously

noted, the amount of octylsilane exposure necessary for formation of a saturated monolayer is highly dependent upon whether the Au(111) substrate has been exposed to ambient atmosphere prior to experimentation in UHV. Presumably, ambient atmosphere exposure temporarily quenches some available reactive sites for octylsilane adsorption, although formation of a saturated octylsilane monolayer is possible on both substrates. The STM experiments presented in this section have been performed on a Au(111) sample exposed to ambient atmosphere ~6.5 min prior to octylsilane exposure in UHV.

Images of a clean Au(111) surface (0 langmuirs) exposed to up to 5 langmuirs of octylsilane are displayed in panels a−c of Figure 4. The herringbone pattern intrinsic to clean Au(111) $23 \times \sqrt{3}$ is faintly discernible in Figure 4a (running vertically through the image). Exposure of the clean Au(111) $23 \times \sqrt{3}$ sample in Figure 4a to 2 langmuirs of octylsilane yields no visible changes (Figure 4b); however, additional octylsilane exposure (5 langmuirs total exposure) yields distinct changes in the sample surface (Figure 4c). Most obvious in Figure 4c is the appearance of darkly contrasted depressions (approximately 0.8 Å in apparent depth and 20−25 Å in apparent width) in the Au(111) $23 \times \sqrt{3}$ surface. The apparent depth of a depressed region is equivalent to the apparent height differential observed for the sinuous ridges relative to the surrounding depressed regions of the condensed, saturated monolayer in Figure 1d. Frequently, the darkly contrasted regions situate on the Au(111) $23 \times \sqrt{3}$ reconstructed surface to form linear rows of surface depressions (e.g., bottom portion of Figure 4c).

The STM images displayed in panels d−f of Figure 4 were collected from a region adjacent to that in Figure 4a−c and represent octylsilane exposures of 5−11 langmuirs. As in Figure 4c, linear rows of darkly contrasted 0.8 Å surface depressions are also apparent in Figure 4d (the Au(111) $23 \times \sqrt{3}$ herringbone surface reconstruction is faintly visible running vertically through the image). Additional octylsilane exposure (8 langmuirs total exposure) results in the broadening of pre-existing, and simultaneous formation of new, surface depressions (Figure 4e). The Au(111) $23 \times \sqrt{3}$ surface reconstruction is barely discernible in Figure 4e, and this image represents the highest octylsilane exposure at which the surface reconstruction is still apparent. Again, further exposure to octylsilane (11 langmuirs total exposure) results in formation of additional surface depressions and broadening of pre-existing features (Figure 4f; tip drift has translated the image area to the right). The streaking along the left edge of Figure 4f is a physical artifact of the STM scanner piezoelectric tube (at the time of image acquisition, the scan tube was maximally extended in the "$-x$" lateral scan direction; the attempted overextension of the scan tube while imaging causes streaking in the image).

A STM movie monitoring incremental octylsilane exposures (20−390 langmuirs) on a single Au terrace displays the rapid and dynamic evolution of octylsilane monolayer surface features. By 20 langmuirs total octylsilane exposure (Figure 5a), growth, and broadening of surface depressions have produced a pattern of sinuous ridges on the substrate surface. The appearance of the first hillock feature in the monolayer surface is apparent at 24 langmuirs total octylsilane exposure (denoted by the arrow in Figure 5b). Panels c−j of Figure 5 track the growth of the hillock feature (which remains on the left-hand side of all the images) and highlight the evolution of additional hillock features for octylsilane exposures of 28−390 langmuirs (tip drift accounts for small variations in feature locations between images). By 40 langmuirs total octylsilane exposure, growth of the initial hillock feature first identified in Figure 5b has ceased and subsequent smaller hillock features proceed to grow in the surrounding area.

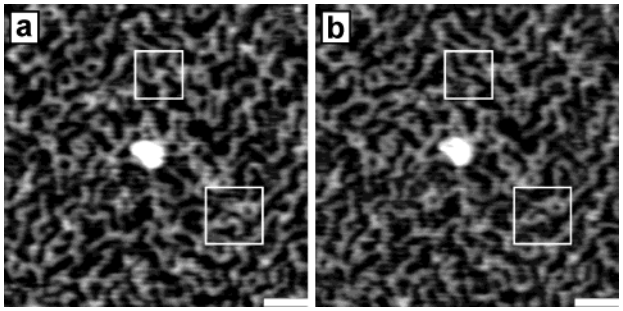


**Figure 6.** Successive UHV-STM images of the same 350 Å × 350 Å region of the unsaturated (32 langmuir total exposure) octylsilane monolayer on Au(111). Over time, the monolayer features exhibit subtle, nearest-neighbor conformation transformations. Two such examples are indicated in the white boxes. (a) Acquired at $\tau_0$; $V_S = -0.99$ V, $I_T = 18$ pA. (b) Acquired at $\tau_0 + 6$ min; $V_S = -0.99$ V, $I_T = 29$ pA.

Close inspection of the STM movie reveals the dynamic behavior of the surface features as the monolayer grows in from partial coverage to the saturated, condensed phase. The dynamic behavior is subtle (but still quite obvious), typically involving small nearest-neighbor topographical modifications. The movie frequently exhibits adjacent sinuous ridges combining, breaking and/or exhibiting lateral "switching" behavior. In addition, ridges frequently form loops and knots that open and close again. Occasionally, small mobile protrusions with an apparent height of ~1.5 Å temporarily appear on the surface that either disappear or become static and enlarge into stationary hillock features. Identical behavior is also apparent in STM images acquired successively over a sample region at a constant submonolayer coverage. Figure 6a displays a 350 Å × 350 Å region of the features formed from submonolayer exposure to octylsilane (32 langmuirs total exposure). Figure 6b displays the same image region in 6a acquired approximately 6 min later. Comparison of panels a and b of Figure 6 yields subtle, nearest-neighbor conformation transformations of the submonolayer features. Two readily apparent examples are indicated in the white boxes in Figure 6.

**3.3. Evolution of Terrace Edge Features.** Recall from Figures 1c and 3 the roughened appearance of Au(111) substrate terrace edges following octylsilane monolayer formation. To best determine the origins of these features, additional in situ UHV-STM experiments monitoring sequential substrate changes as a function of increasing octylsilane exposure have been performed for an image region containing two individual Au terraces. Figure 7 displays static snapshots for representative octylsilane exposure amounts (in langmuirs); however, the data are best viewed dynamically in movie format. The STM experiments presented in this section have been performed on a Au(111) sample exposed to ambient atmosphere ~6.5 min prior to octylsilane exposure in UHV. Figure 7a displays two substrate terraces with the ascending terrace edge running horizontally across the image. The images presented in Figure 7 have been plane and slope subtracted, minimizing the vertical step height differences, to best visualize the monolayer features across both terraces. This image processing procedure artificially produces a shadowing effect along the terrace edge and highlights the step edge features. As previously noted for

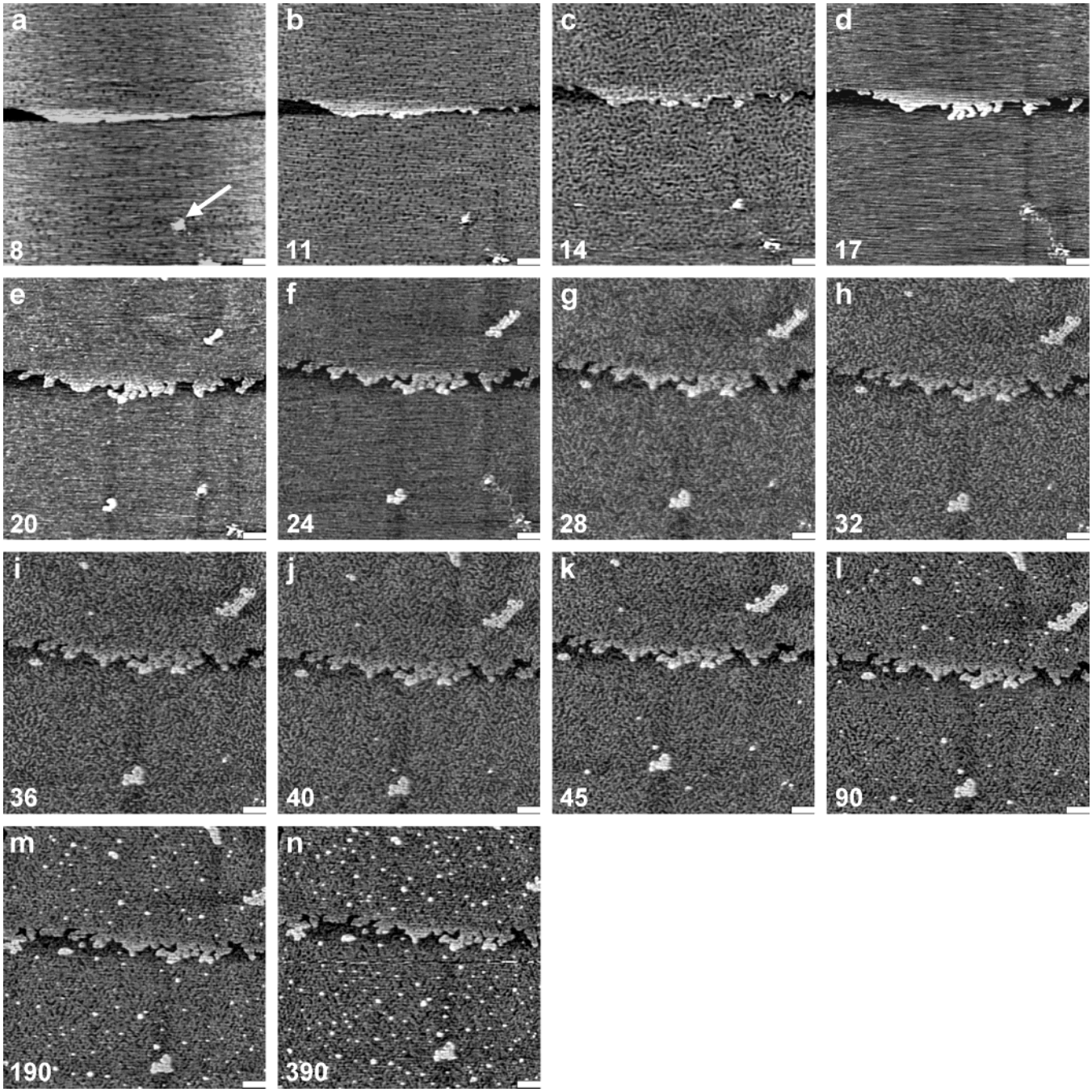


**Figure 7.** Incremental in situ UHV-STM images of two individual Au(111) terraces as a function of increasing octylsilane exposure (indicated in the lower left corner). The Au(111) sample was exposed to ambient atmosphere ~6.5 min prior to octylsilane exposure. All images are 1220 Å × 1220 Å in area and were acquired with $V_S = -1$ V and $I_T = 5-35$ pA. The white scale bar in the bottom right corner of each image signifies 100 Å.

Ⓦ A STM animation showing increasing octylsilane exposure, 8 to 390 langmuirs, in GIF format is available.

sample exposure to 8 langmuirs of gaseous octylsilane (Figure 4e), darkly contrasted 0.8 Å surface depressions are also apparent in Figure 7a. Additionally, the terrace edge already appears slightly roughened at this coverage regime. The arrow in Figure 7a denotes a pre-existing surface defect (most likely a carbonaceous contaminate as a result of the Au(111) substrate preparation procedure) that serves as a registry point in subsequent images presented in Figure 7 (the defect remains in the lower right-hand corner of each image). As the sample is subject to increasing octylsilane exposure, the step edge undergoes dramatic topographical transformations. Most obvious in Figure 7 is the appearance and incremental growth of fingerlike structures protruding laterally outward from the original step edge. The apparent heights of the new features are equivalent to and indistinguishable from that of the original single-step Au terrace (~2.5 Å). Significant growth of the step edge features occurs prior to formation of the static interstitial hillock features (the first of which appear at 20 langmuirs total octylsilane exposure, denoted by arrows in Figure 7e); however, additional growth of the terrace edge features continues throughout subsequent dosage increments. In addition, the two initial static hillock features identified in Figure 7e significantly enlarge in subsequent dosage increments. By 45 langmuirs total octylsilane exposure (Figure 7k), growth of the step edge and initial hillock features identified in Figure 7e has ceased. Subsequent octylsilane exposures result in forma-

tion and enlargement of additional smaller (20−40 Å wide) interstitial hillock features in the surrounding area (Figure 7k−n).

## 4. Discussion

The STM data presented in this paper display the complex and dynamic behavior of octylsilane monolayer formation on Au(111) $23 \times \sqrt{3}$. In this section, a thorough interpretation of the STM data is presented. In addition, the octylsilane monolayer pattern formation mechanism is addressed.

**4.1. Origin and Behavior of Au Islands.** Low coverage STM data indicate adsorption of octylsilane molecules is characterized by the appearance of 0.8 Å depressions in the Au(111) $23 \times \sqrt{3}$ surface (Figure 4). Additional octylsilane exposure results in the broadening of pre-existing, and simultaneous appearance of new, depressed regions. This behavior continues until a pattern of sinuous ridges is created and concludes with the appearance of static interstitial island features ∼2.5 Å in apparent height. The presence of islands indicates the $23 \times \sqrt{3}$ surface reconstruction has fully relaxed to form Au(111) $1 \times 1$, as commonly observed during alkanethiol self-assembled monolayer formation.[51,52] Similar island features have also been observed in STM studies employing electrochemical methods to lift the Au(111) $23 \times \sqrt{3}$ surface reconstruction.[53,54] The Au(111) $23 \times \sqrt{3}$ surface contains ∼4.3% excess Au atoms, with each $1 \times 23$ primitive unit cell of the reconstructed surface containing one extra Au atom.[46−49] Octylsilane monolayer formation results in ejection and nucleation of the excess surface Au atoms and relaxation of the $23 \times \sqrt{3}$ surface reconstruction. Migration and nucleation of surface adatoms create small Au islands. The percentage of the image area covered by the Au islands (7% in Figure 2a, with a range of 4−10% typically observed in the STM images) is consistent with ejection of more than one atom per unit cell as suggested by Poirier for thiophenol monolayer formation on Au(111).[52] However, this number is a lower bound for gold adatom generation as it does not include adatoms which have combined with terrace edges. In situ UHV-STM experiments monitoring sequential substrate changes as a function of increasing octylsilane exposure highlight the evolution of the Au adatoms and the effect they have upon diffusion to terrace edges.

Figures 5 and 7 dramatically display the diffusion effects of the Au adatoms on step edge roughening and island formation. Recall the STM movies display temporary surface protrusions ∼1.5 Å in apparent height that either disappear or become static and enlarge into stationary islands. These features are consistent with individual mobile Au adatoms as previously observed during mercaptohexanol monolayer formation on Au(111).[52] As noted by Poirier, the ∼1.0 Å apparent height differential of an isolated Au adatom relative to single-step Au(111) is likely due to the difference in electronic state densities between a single atom and a close-packed island comprised of numerous Au atoms.[52] Similar apparent height differences have also been observed for Pt adatoms on Pt(111).[55] Some of the mobile surface Au adatoms diffuse to terrace edges and adsorb. Fingering of the terrace edge indicates minimal adatom mobility along the step edge. This aggregation structure is clearly evident in Figure 7. The appearance of stable Au islands at submonolayer exposures (≤24 langmuirs; Figures 5b and 7e) likely result from localized pinning defects on the underlying substrate that effectively trap mobile Au atoms in that region. Diffusion and adsorption of additional mobile Au adatoms expand the islands in the same manner as the terrace edges. Subsequent octylsilane exposure increases the monolayer surface density and reduces the mobility of the Au adatoms, resulting in nucleation of 20−40 Å diameter Au islands observed in the saturated monolayer surface. Recall $I-V$ STS data of the saturated monolayer does not distinguish significant differences between the Au islands and the surrounding monolayer features, indicating the Au islands also have identical octylsilane coverage (since bare Au islands on top of the monolayer would exhibit different electronic signatures). Consequently, the islands are accurately construed as small, single-step Au terraces underneath the chemisorbed monolayer. Octylsilane coverage is also inferred from the sinuous ridge features apparent on the Au islands identical to those in the surrounding octylsilane monolayer regions (Figures 5 and 7). Recently, variable energy XPS studies of alkylsilane monolayers meausured ∼96% octylsilane monolayer coverage on the Au(111) substrate.[31] The STM and STS data support this value as at least a lower boundary.

A quantitative analysis of the growth of the step edge and the island formation allows the number of gold atoms ejected per $23 \times \sqrt{3}$ unit cell to be assessed. Gold island coverage in Figure 7, panel n, is ∼5%. Addition of gold to the step edge was quantified by comparing panels a and k from Figure 7. The increase in area of the step edge is equal to ∼7% of the image area. Thus, the combined total of additional gold on the surface at saturation coverage of octylsilane is ∼12%. The Au(111) $23 \times \sqrt{3}$ surface reconstruction contains 4.3% excess gold atoms or one extra atom per unit cell. The remaining ∼7.7% additional gold on the surface is consistent with ca. two more gold atoms ejected per unit cell. In summary, chemisorption of a saturated monolayer of octylsilane onto the Au(111) $23 \times \sqrt{3}$ surface reconstruction results in the breaking of the reconstruction and the ejection of ca. three gold atoms per unit cell.

**4.2. Origin and Behavior of the Saturated Monolayer Features.** Thus far, the origin and behavior of the Au islands during octylsilane monolayer formation have been addressed. However, the origin of the remaining monolayer features (i.e., the sinuous ridges and surrounding depressed regions) has not been discussed. Recall, low coverage STM data indicate octylsilane adsorption is characterized by the appearance of 0.8 Å depressions in the Au(111) $23 \times \sqrt{3}$ surface. Consequently, one might hypothesize the depressions in the saturated monolayer, constituting ∼45% of the surface, represent regions of appreciable octylsilane coverage whereas the light areas, the elevated sinuous ridges comprising ∼48% of the surface, indicate areas devoid of octylsilane coverage. However, recent variable coverage XPS data examining the Si 2p and Au 4f features measured ∼96% octylsilane monolayer coverage on the Au(111) substrate and therefore effectively rules out the above hypothesis.[31]

Frequently, the pattern formation mechanism of alkanethiol SAMs on Au(111) is explained as a consequence of alkyl chain crystallization and/or variations in alkyl chain angle or orientation.[34,56−58] One might also conclude the octylsilane monolayer features are the result of varying octylsilane alkyl chain phases. Subtle variations in alkyl chain angle or orientation may yield differing apparent heights of octylsilane monolayer features as observed by

(51) Poirier, G. E.; Pylant, E. D. *Science* **1996**, *272*, 1145−1148.
(52) Poirier, G. E. *Langmuir* **1997**, *13*, 2019−2026.
(53) Tao, N. J.; Lindsay, S. M. *J. Appl. Phys.* **1991**, *70*, 5141−5143.
(54) He, Y.; Borguet, E. *J. Phys. Chem. B* **2001**, *105*, 3981−3986.
(55) Zeppenfeld, P.; Lutz, C. P.; Eigler, D. M. *Ultramicroscopy* **1992**, *42−44*, 128−133.

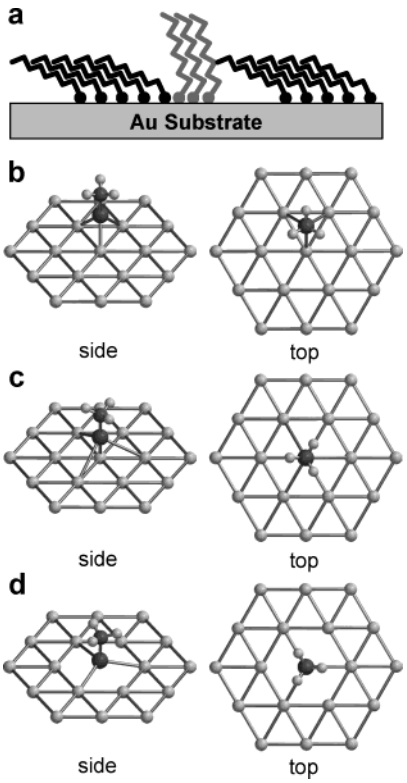


**Figure 8.** Potential octylsilane adsorption models. (a) Molecular adsorption with localized domains of variations in alkyl chain angle or orientation. Molecular adsorption on Au(111) in (b) a 3-fold hollow site, (c) an atop site yielding pentacoordinate Si, and (d) a surface vacancy site. For clarity, the chemisorbed octylsilane molecule is represented by $CH_3SiH_3$.

STM (Figure 8a).[56] However, STM data of methanethiol ($CH_3SH$) SAM formation on Au(111) suggests otherwise. Chemisorption of methanethiol onto Au(111) $23 \times \sqrt{3}$ produces monolayer domains exhibiting a "striped" phase.[59] The appearance of "striped" phases in alkanethiol monolayers is typically attributed to alkyl chain−chain interactions and/or crystallization. Considering the methanethiol SAM lacks extended alkyl chains, the STM data suggest Au−S interactions, not alkyl chain interactions, predominantly determine alkanethiol monolayer features.[59] Recent STM studies investigating methanethiol and octanethiol ($C_8H_{17}SH$) SAM formation on Cu(111) derive a similar conclusion.[60,61] Instead, interfacial Cu−S interactions are proposed to predominantly determine the SAM pattern formation on Cu(111). Therefore, interfacial Au−Si interactions, not alkyl chain interactions, are proposed to predominantly determine the structural features of the octylsilane monolayer. Consequently, Figure 8a is effectively ruled out as a potential source of the observed monolayer pattern.

XPS and RAIRS characterization of the octylsilane monolayer indicates octylsilane chemisorbs to Au(111) via cleavage of the three Si−H bonds and subsequent formation of covalent Si−Au bonds, leaving the molecule standing upright on the substrate.[30,31] Consideration of the spectroscopic data yields three potential molecular chemisorption models for octylsilane on Au(111). One model involves molecular adsorption in the Au(111) "3-fold hollow" site (Figure 8b) while the second and third models entail adsorption at atop sites (Figure 8c,d). Parts b and d of Figure 8 orient the molecule in a conformation conducive to three Au−Si bonds, whereas Figure 8c contains four Au−Si bonds and a pentacoordinate Si atom.

Geometric considerations involving a tetrahedral Si atom indicate both parts b and d of Figure 8 are incommensurate with the Au(111) lattice and would require substantial surface reconstruction. Presuming tetrahedral angles about the Si atom and Si−Au bond lengths equal to the sum of the covalent radii (2.44 Å), the Au−Au distances for a $RSiAu_3$ moiety are required to be ∼4 Å. This distance does not match the Au−Au (2.68 Å) or Au···Au (4.68 Å) first and second neighbor distances, respectively. Mechanics calculations of parts b and d of Figure 8 predict unreasonably high energies if the Au(111) lattice is held rigid. Similarly, pentacoordinate bonding models involving a trigonal bipyramidal or square pyramidal Si atom also yield a Au−Au distance incommensurate with the gold lattice. Therefore, the most reasonable chemical bonding models ultimately require substantial reconstruction of the Au surface. Recent density functional theory (DFT) calculations by Hammer et al. suggest an adsorbate-induced surface reconstruction of the Au(111) surface minimizes surface strain and stabilizes molecular adsorption.[62] For tetrahedral silicon, this can be accomplished via expansion of the Au−Au distances in the 3-fold hollow site (Figure 8b) or via ejection of a Au atom and contraction of the Au···Au second neighbor distances (Figure 8d). An adsorption model involving a pentacoordinate Si atom (Figure 8c) requires both contraction of the Au···Au second neighbor distances and dislocation of the center Au atom further downward into the gold lattice. In addition to the models illustrated, pentacoordinate models in which the Si atom is found in the bridge binding site with either a butterfly or square pyramidal bonding configuration are also possible. Pentacoordinate Si has recently been proposed for the interaction of trimethylsilyl headgroups to Au(111).[35,36] The adoption of any two of these binding models is consistent with the two-phase surface pattern observed in the octylsilane monolayer. The adsorption models depicted in parts c and d of Figure 8 are a compelling pair considering they differ only by the ejection of the central gold atom (vida infra).

Recall, STM data monitoring sequential changes in substrate features as a function of octylsilane exposure first indicate the appearance of small, depressed regions after approximately 5 langmuirs of exposure. However, the STM data do not rule out significant octylsilane adsorption at lower exposures. Scanning tunneling spectroscopy $I-V$ measurements of the area-averaged tunnel junction display an increase in electrical resistance with increasing octylsilane exposure and suggest 85% of the surface is covered after a 5 langmuir exposure and >90% after 14 langmuirs exposure (Figure 9). The decay constant for the resistance change is 2.5 langmuirs and the exponential fit between the junction resistance and exposure (Figure 9b) provides direct evidence for molecular adsorption well before the observation of depressed regions in the STM images. Instead, the depressed regions only become evident as the density of adsorbed octylsilane molecules increases.

(56) Bumm, L. A.; Arnold, J. J.; Dunbar, T. D.; Allara, D. L.; Weiss, P. S. *J. Phys. Chem. B* **1999**, *103*, 8122−8127.
(57) Zeng, C.; Li, B.; Wang, B.; Wang, H.; Wang, K.; Yang, J.; Hou, J. G.; Zhu, Q. *J. Chem. Phys.* **2002**, *117*, 851−856.
(58) Li, B.; Zeng, C.; Li, Q.; Wang, B.; Yuan, L.; Wang, H.; Yang, J.; Hou, J. G.; Zhu, Q. *J. Phys. Chem. B* **2003**, *107*, 972−984.
(59) Dishner, M. H.; Hemminger, J. C.; Feher, F. J. *Langmuir* **1997**, *13*, 2318−2322.
(60) Driver, S. M.; Woodruff, D. P. *Surf. Sci.* **2000**, *457*, 11−23.
(61) Driver, S. M.; Woodruff, D. P. *Langmuir* **2000**, *16*, 6693−6700.
(62) Molina, L. M.; Hammer, B. *Chem. Phys. Lett.* **2002**, *360*, 264−271.

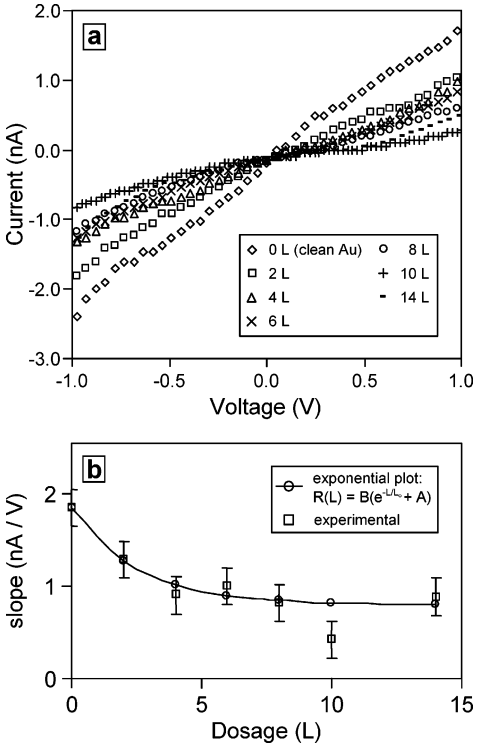


**Figure 9.** (a) Scanning tunneling spectroscopy (STS) $I-V$ data monitoring the change in electrical resistance of the area-averaged tunnel junction as a function of octylsilane exposure. (b) An exponential fit of the tunnel junction resistance versus dosage amount indicates ~85% octylsilane coverage on the Au(111) substrate following 5 langmuirs of octylsilane exposure. The parameters used for the exponential fit are $A = 0.8$ and $B = 1.1$ nA/V.

Similar features have been previously observed in STM data examining Ni and Na place exchange on Au(111).[63,64] The STM data and movies presented in Figures 2, 5, and 7 clearly indicate ejection of Au surface atoms occurs during octylsilane monolayer formation. Furthermore, Figure 2 suggests the ejection of more than one Au atom per unit cell based upon the percentage of Au island surface coverage. Such an occurrence would yield a defected substrate surface characterized by numerous atomic vacancies. However, "vacancy island" formation is *never* observed during octylsilane monolayer formation. Whereas alkanethiol SAM formation on Au(111) frequently produces ~2.5 Å (the monatomic step height of Au) deep vacancy pits in the underlying substrate,[8,51,52] only 0.8 Å depressions are ever observed in the octylsilane monolayer surface. It is possible Au/octylsilane Si place exchange occurs at substrate vacancy sites produced as a result of surface Au atom ejection. This hypothesis assumes the 0.8 Å depressed regions correspond to areas where surface Au atom ejection followed by octylsilane adsorption has occurred. Consequently, the simultaneous presence of two octylsilane adsorption phases is implied: adsorption at an atop site yielding pentacoordinate Si (Figure 8c) and adsorption of a tetracoordinate Si in a substrate vacancy site (Figure 8d). This hypothesis is supported by recent experimental[60,61] and theoretical[62] investigations of analogous alkanethiol SAM formation on Cu(111) and Au(111) surfaces, respectively. Both theory and experiment conclude ejection of substrate surface atoms occurs during alkanethiol SAM formation. DFT calculations indicate a 0.8 eV net stabilization in adsorption energy on Au(111)[62] and experiments conclude substrate atomic place exchange occurs at Cu(111) surface vacancy sites.

Qualitative analysis of the octylsilane monolayer features provides instructive information concerning possible origins of the monolayer pattern. The octylsilane monolayer surface vaguely resembles numerous self-assembly systems including block copolymers and polymer blends,[65−67] metal alloys,[68] ferromagnetic films,[69] and a variety of other two- and three-dimensional chemical and physical systems.[70] However, Figure 1d bears strongest resemblance to theoretical investigations of spinodal decomposition[71] and monolayer pattern formation dynamics on a solid surface.[43−45,72] Simulations examining two-phase monolayer self-assembly dynamics on an elastic substrate with isotropic surface stress (such as the reconstructed Au(111) $23 \times \sqrt{3}$ surface) share a number of similarities with octylsilane monolayer formation.[43−45] The simulations conclude monolayer formation on an elastic substrate sequentially entails (1) phase separation, (2) size selection, and (3) spatial ordering.[43−45]

Recall parts c and d of Figure 8 suggest the presence of two octylsilane adsorption phases. It is possible octylsilane monolayer pattern formation results from spinodal decomposition of the two adsorption phases. To test the feasibility of this pattern formation mechanism, simulations of two-phase monolayer self-assembly dynamics on a substrate with isotropic surface stress have been performed. Whereas previous simulations have investigated pattern formation starting from a fixed concentration of the two phases,[43−45] the simulation results presented here investigate monolayer pattern formation as a function of increasing the concentration of one phase relative to the other. In doing so, the simulation mimics the incremental dosing procedure of the STM experiments which indicate the concentration of octylsilane adsorption phase in Figure 8d increases as a function of continued octylsilane exposure.

Simulation results have been compiled in movie format for easy comparison to the experimental STM movies. In the simulation, the two adsorption phases in parts c and d of Figure 8 are represented by light and dark features, respectively. Individual images from the simulation movie are presented in Figure 10. Early in the simulation, the appearance of dark "spots" is apparent. As the concentration of the dark phase is increased, the dark spots simultaneously increase in number and size and quickly segregate to form a pattern of nanoscale interwoven stripes. The width and overall pattern of the interwoven stripes rapidly stabilize following this step. As time progresses, the interwoven stripes exhibit subtle nearest-neighbor conformation transformations. Adjacent stripes combine and break to form loops and/or knots. The simulation closely mimics the STM data displaying the evolution of octylsilane monolayer features. Furthermore, the dynamic behavior of the simulated interwoven stripes closely resembles that observed for the sinuous ridges in

(63) Barth, J. V.; Behm, R. J.; Ertl, G. *Surf. Sci.* **1995**, *341*, 62−91.
(64) Meyer, J. A.; Baikie, I. D.; Kopatzki, E.; Behm, R. J. *Surf. Sci.* **1996**, *365*, L647-L651.
(65) Park, M.; Harrison, C.; Chaikin, P. M.; Register, R. A.; Adamson, D. H. *Science* **1997**, *276*, 1401−1404.
(66) Karim, A.; Slawecki, T. M.; Kumar, S. K.; Douglas, J. F.; Satija, S. K.; Han, C. C.; Russell, T. P.; Liu, Y.; Overney, R.; Sokolov, O.; Rafailovich, M. H. *Macromolecules* **1998**, *31*, 857−862.
(67) Keblinski, P.; Kumar, S. K.; Maritan, A.; Koplik, J.; Banavar, J. R. *Phys. Rev. Lett.* **1996**, *76*, 1106−1109.
(68) Plass, R.; Last, J. A.; Bartelt, N. C.; Kellogg, G. L. *Nature* **2001**, *412*, 875.
(69) Giess, E. A. *Science* **1980**, *208*, 938−943.
(70) Seul, M.; Andelman, D. *Science* **1995**, *267*, 476−483.
(71) Cahn, J. W.; Hilliard, J. E. *J. Chem. Phys.* **1958**, *28*, 258−267.
(72) Schuster, R.; Thron, D.; Binetti, M.; Xia, X.; Ertl, G. *Phys. Rev. Lett.* **2003**, *91*, 066101.

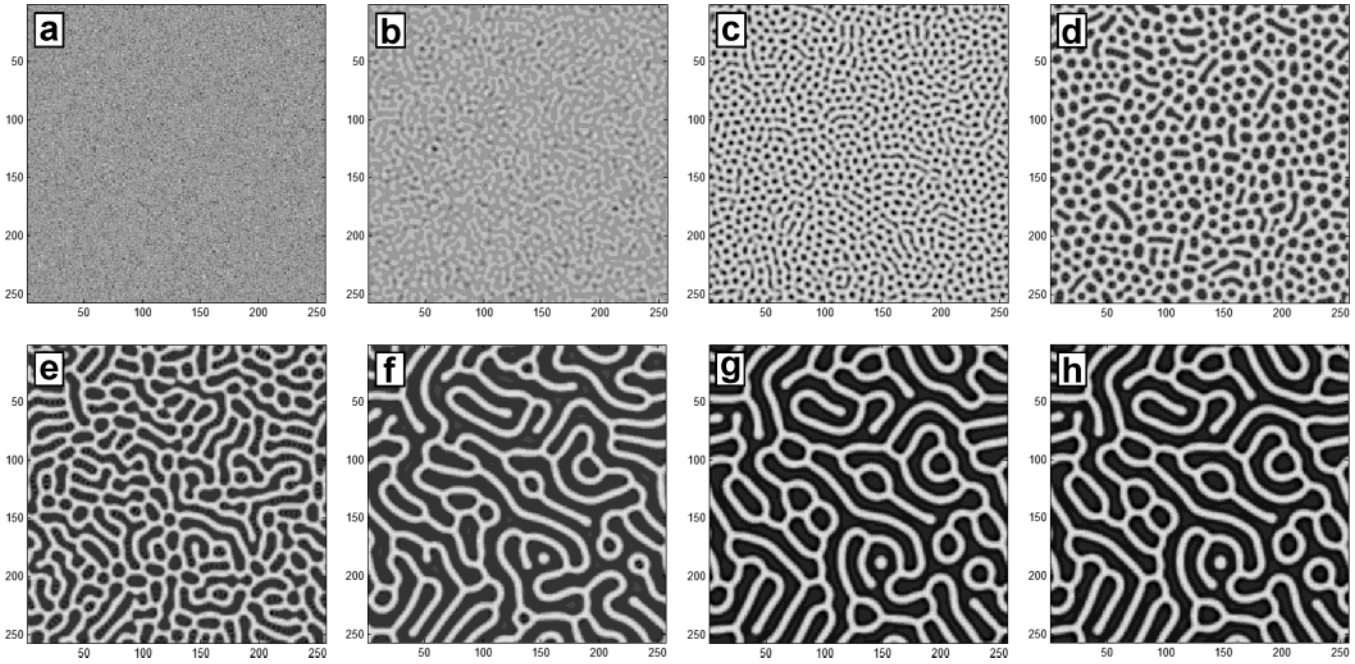


**Figure 10.** Theoretical simulation investigating the self-assembly and pattern formation dynamics of a two-phase monolayer on a solid substrate. The percentage of one phase increases relative to the other from (a) to (h). The length scale of the resulting pattern in (f) is 60 Å.

Ⓦ Simulation results in animation (GIF file) are available.

the STM movies examining octylsilane monolayer formation. The large degree of correlation between the theoretical simulations and the experimental data suggests the octylsilane monolayer pattern results from a three-step self-assembly process involving separation, size selection, and spatial ordering of the two adsorption phases. Furthermore, the simulations indicate the monolayer pattern formation is driven by surface strain.

An important feature of the simulations is the emergence of an asymptotic length scale for the pattern features, which allows quantitative comparison to the experimental data. The model produces two fundamental length scales: $l$, the domain feature size, and $b$, the scale of the transition region between the two monolayer phases. By use of parameters for the elastic modulus of Au and the relative binding energy difference between the two adsorption phases (parts c and d of Figure 8), the two length scales in the model are calculated to be $l \approx 60$ Å and $b \approx 6$ Å, in excellent agreement with the experimental data. This indicates the spatial extent of the pattern is appropriate for the physical mechanism of elastically driven phase separation in addition to the comparable temporal evolution exhibited between the simulation model and experimental data. Furthermore, the model predicts an abrupt (i.e., atomic in scale) transition region between phases, $b$. Note this molecular assembly mechanism only considers the interaction of surface and interfacial species and does not invoke potential effects of the alkyl chains. Therefore, the simulation suggests the monolayer features solely result from surface Au−Si interactions, not alkyl chain interactions.

## 5. Summary and Conclusions

UHV-STM data investigating octylsilane monolayer formation on Au(111) have been presented. Octylsilane monolayer formation relaxes the Au(111) $23 \times \sqrt{3}$ surface reconstruction and ejects surface Au adatoms. The Au adatoms diffuse and either adsorb onto terrace edges (epitaxially extending the stepedge laterally outward) or become trapped and nucleate Au islands at monolayer saturation coverage. STS data of the saturated monolayer suggest uniform monolayer coverage across the Au(111) substrate. Theoretical and experimental data suggest the presence of two octylsilane adsorption phases within the chemisorbed monolayer: adsorption at an atop site yielding a pentacoordinate Si unit and adsorption in a surface vacancy site yielding a tetracoordinate Si unit. In situ UHV-STM characterization of octylsilane monolayer formation closely resembles theoretical simulations examining two-phase monolayer self-assembly dynamics on an elastic substrate with isotropic surface stress. The simulations suggest the monolayer pattern and features result from a spinodal decomposition mechanism involving a three-step self-assembly process of surface phase separation, size selection, and spatial ordering of the two adsorption phases. In addition, the simulations produce the characteristic ~60 Å length scale apparent in STM images of the octylsilane monolayer pattern. The octylsilane monolayer pattern is dramatically different from that previously observed in analogous alkanethiol SAM systems and is unique to the field of chemisorbed organic layers on surfaces. The combination of theoretical and experimental data suggests the complex octylsilane monolayer pattern results from strain-mediated spinodal decomposition of two different molecular adsorption phases and the alkyl chains do not play a significant role in evolution of the monolayer pattern.

**Acknowledgment.** RHK Technology, Inc., and the National Science Foundation (DMR-0093641) are gratefully acknowledged for support of this work. D.R.F. thanks the NSF for an IGERT fellowship (DGE-9972776). J. A. Hessler is gratefully acknowledged for her assistance in preparation of Figure 2. T. M. Owens is thanked for numerous helpful discussions. We thank J. E. Carey for suggesting consideration of a spinodal decomposition model.

LA0360916